The Mean-Meridional Transport Circulation of the Troposphere in an Idealized GCM

KENNETH P. BOWMAN AND GORDON D. CARRIE

Department of Atmospheric Sciences, Texas A&M University, College Station, Texas

(Manuscript received 11 September 2000, in final form 26 October 2001)

ABSTRACT

Large numbers of particle trajectories are used to characterize the mean-meridional transport circulation of an idealized general circulation model (GCM). The GCM has a uniform land surface, no topography or land–sea contrasts, and no seasonal cycle. The trajectories are analyzed using both Lagrangian-mean statistics and an approach based on the Green's function of the tracer transport equation. It is shown that the distribution of particle trajectories provides an estimate of the ensemble-mean Green's function for the inviscid transport equation. Lagrangian means have a number of problems that render their interpretation difficult, including boundary effects and selection of the appropriate averaging period. The Green's function, on the other hand, provides a quantitative description of the transport circulation that is easy to visualize and interpret. The results demonstrate that within the idealized model the atmosphere can be divided into three parts: the Southern Hemisphere extratropics, the Tropics, and the Northern Hemisphere extratropics. Climatologically, particle dispersion within each part of the atmosphere is rapid, while exchange between the different parts is much slower. There is a semipermeable transport barrier between the Tropics and extratropics. The interhemispheric exchange rate in the model is toward the slower end of estimates from observations, possibly due to the higher degree of zonal symmetry in the model.

1. Introduction

Human activities are having increasing effects on the global atmosphere. Understanding and predicting the effects of anthropogenic substances released into the atmosphere will require understanding the interrelated roles of transport, radiation, and chemistry. Most man-made substances added to the atmosphere are present in small concentrations and have little direct effect on atmospheric motions. It is often useful, therefore, to treat these substances as though they are passively transported by the atmospheric circulation. Even in the ideal case of passive, long-lived tracers, however, the complexity of atmospheric motion makes understanding and predicting transport very difficult. At present, many aspects of the transport circulation in the atmosphere are poorly understood.

The classic approach to studying the general circulation of the atmosphere has been through analysis of Eulerian statistics (e.g., Oort and Rasmusson 1971). Simulations made with global climate models are often compared to the observed circulation by using Eulerian statistics such as zonal means and eddy variances. Similarly, simulations of trace species distributions are often evaluated by computing such quantities as time-mean zonal-mean cross sections. It is now understood, however, that transport by the Eulerian-mean circulation is largely cancelled by eddy transport, so the mean transport circulation must, in general, be quite different from the Eulerian-mean circulation (Boyd 1976; Andrews and McIntyre 1976; Andrews and McIntyre 1978b; Dunkerton 1978; Andrews 1983; Plumb and Mahlman 1987). Therefore, the conventional Eulerian-mean circulation may not provide much insight into atmospheric transport problems. Some of the problems with Eulerian-mean methods can be avoided by the use of isentropic coordinates or by defining a residual-mean circulation in the transformed Eulerian-mean framework (e.g., Andrews et al. 1987; Townsend and Johnson 1985; Stone et al. 1999; Held and Schneider 1999), but the residual-mean circulation may not capture all of the transport effects of the eddies.

Another approach to the problem of transport is through Lagrangian methods. While it is possible to develop dynamical models in a Lagrangian framework, the label Lagrangian generally refers to kinematic studies. That is, the atmospheric velocity field is known at some resolution from a model or from observations. That velocity field is used to compute the trajectories of hypothetical massless air parcels in the evolving flow field; and the trajectories are analyzed to study, transport, mixing, etc.

Lagrangian methods have proven to be very useful in understanding stratospheric transport problems (Hsu

Corresponding author address: Dr. Kenneth P. Bowman, Department of Atmospheric Sciences, 3150 Texas A&M University, College Station, TX 77843-3150.
E-mail: k-bowman@tamu.edu

1980; Matsuno 1980; Kida 1983; Austin and Tuck 1985; Schoeberl et al. 1992; Bowman 1993; Fisher et al. 1993; Pierce and Fairlie 1993; Chen 1994; Sutton et al. 1994; Bowman 1996). Schoeberl et al. (2000) have recently reviewed some of the strengths and weakness of Lagrangian approaches to understanding trace gas distributions in the stratosphere. Although Lagrangian kinematic analysis methods have received widespread use in the stratosphere and for the interpretation of tropospheric field experiments, with the exception of a few studies, trajectories have not been applied extensively to study the global transport circulation in the troposphere (e.g., Kida 1983; Pierrehumbert and Yang 1993). As observations and simulations of the chemistry of the troposphere advance, there is a need for methods to characterize and evaluate the transport circulation. In this paper we compare two possible methods for the quantitative analysis of the large-scale transport circulation and illustrate those methods with calculations based on a simulation with an idealized general circulation model (GCM).

2. Background

a. Lagrangian-mean circulation

Transport studies are concerned with the pathways and mechanisms by which the atmosphere carries atmospheric properties from one location to another. Because of this, Lagrangian methods, which consider the trajectories of individual air parcels, are a natural way to study the transport circulation. If the velocity field is known, then the trajectory of a hypothetical massless parcel of air can be found from the kinematic equations of motion,

$$\frac{d\mathbf{x}'}{dt} = \mathbf{v}(\mathbf{x}', t) \quad \text{and} \quad \mathbf{x}'(0) = \mathbf{x}'_0, \tag{1}$$

where $\mathbf{x}'$ is the position of the parcel as a function of time t, $\mathbf{v}$ is the velocity, and $\mathbf{x}'_0$ is the initial location of the parcel at $t = 0$. (Primes are used to explicitly denote a particle trajectory.) Given an ensemble of many realizations of the velocity field, (1) can be solved for each member of the ensemble. Lagrangian statistics can then be computed for the ensemble of trajectories. The mean position of the particles as a function of time is $\langle \mathbf{x}'(t) \rangle$, where angle brackets indicate the ensemble average. The ensemble-mean velocity of the parcels is

$$\frac{\langle \mathbf{x}'(t) - \mathbf{x}'_0 \rangle}{t}. \tag{2}$$

The variance of the particles' positions around the mean position

$$\langle (\mathbf{x}' - \langle \mathbf{x}' \rangle)^2 \rangle \tag{3}$$

provides a measure of the dispersion of the particles. These statistics, which typically depend on $\mathbf{x}'_0$ and t, provide one approach to defining a transport climatology of the atmosphere.

The Lagrangian statistics have several important properties. First, as $t \to 0$, the mean particle velocity converges to the average velocity at the initial location $\langle \mathbf{v}(\mathbf{x}'_0, 0) \rangle$ (i.e., the Eulerian ensemble–mean velocity). Second, in an unbounded domain the mean position and the variance can increase without limit; but in a bounded domain such as the earth's atmosphere, air parcels eventually mix throughout the volume. As parcels mix throughout a finite volume, the mean position tends toward the ''center'' of the volume, the velocity tends to zero, and the variance tends to a constant.

Boundaries can also have important effects at short times. Most notably, if $\mathbf{x}'_0$ is near a boundary, parcels can disperse only into the interior of the fluid, not across the boundary. As a result, parcel distributions are frequently asymmetric (skewed) and the mean parcel velocity, which can be strongly affected by a small number of parcels that disperse a large distance, tends to be directed away from the boundary into the interior of the fluid (Andrews and McIntyre 1978a; Plumb and Mahlman 1987). This asymmetry could be characterized by computing third moments of the parcel distributions, but, as we shall show below, it is often more useful to study the complete distribution of parcels rather than to try to represent the distribution with a small number of parameters (i.e., the first few moments). Therefore, Lagrangian-mean quantities in bounded domains are useful only at intermediate times, which means that the choice of averaging interval is crucial. Because the appropriate averaging interval may vary from place to place, producing consistent pictures of the Lagrangian velocity field can be problematic.

b. Green's function method

Because Lagrangian statistics have important limitations, it is useful to consider other approaches to representing the transport circulation. Consider the continuity equation for a conserved trace species

$$\frac{\partial s}{\partial t} + L_{\mathbf{x},t}[s] = 0, \qquad s(\mathbf{x}, 0) = s_0(\mathbf{x}), \tag{4}$$

where $\mathbf{x} = (x, y, \ldots)$ is position, t is time, and $s(\mathbf{x}, t)$ is the mass mixing ratio of the tracer. The transport operator $L_{\mathbf{x},t}[s]$ could be, for example, the advection operator $\mathbf{v} \cdot \nabla s$ or the advection–diffusion operator, $\mathbf{v} \cdot \nabla s - \kappa \nabla^2 s$. If $\mathbf{v}$ and, if necessary, κ are known, then (4) is a linear differential equation for s.

A formal solution to (4) can be found through a Green's function approach (Hall and Plumb 1994; Holzer 1999). The Green's function is the solution to (4) for all possible δ-function initial conditions (all $\mathbf{x}_0$); that is,

$$\frac{\partial G}{\partial t} + L_{\mathbf{x},t}[G] = 0, \qquad G(\mathbf{x}, \mathbf{x}_0, 0) = \delta(\mathbf{x} - \mathbf{x}_0). \tag{5}$$

Given G, the solution to (4) for an arbitrary initial condition $s_0(\mathbf{x})$ can be found from

$$s(\mathbf{x}, t) = \int_{\mathbf{x}_0} s_0(\mathbf{x}_0) G(\mathbf{x}, \mathbf{x}_0, t)\, d\mathbf{x}_0. \quad (6)$$

This approach can be easily extended to find the climatological transport properties of the atmosphere. Given an ensemble of $\mathbf{v}$ fields, as in the previous section, (4) can be solved repeatedly for the same initial condition. The ensemble-mean solution $\langle s \rangle$ is found by taking the ensemble mean of (6), which yields

$$\langle s(\mathbf{x}, t) \rangle = \int_{\mathbf{x}_0} s_0(\mathbf{x}_0) \langle G(\mathbf{x}, \mathbf{x}_0, t) \rangle\, d\mathbf{x}_0. \quad (7)$$

Therefore, for a specified initial distribution $s_0(\mathbf{x})$ the ensemble-mean tracer distribution at future times can be found from the ensemble-mean Green's function. More importantly, perhaps, $\langle G \rangle$ provides a quantitative description of the climatological transport of a trace species from an initial location $\mathbf{x}_0$ throughout the atmosphere. Thus, $\langle G \rangle$ is an alternative way to represent the transport circulation of the atmosphere.

As might be expected, there is a close connection between the solutions to (1) and the Green's function in the nondiffusive case, that is, where $L[s] = \mathbf{v} \cdot \nabla s$. The Green's function for (4) is

$$G(\mathbf{x}, \mathbf{x}_0, t) = \delta(\mathbf{x} - \mathbf{x}'(\mathbf{x}_0', t)), \quad (8)$$

where $\mathbf{x}'(\mathbf{x}_0', t)$ is the solution to the trajectory equation (1). This occurs because the trajectories are simply the characteristics of (4) in the nondiffusive case. An alternative way of stating this result is that, because there is no diffusion, the transport operator simply advects the δ-function initial condition without changing its shape. The path followed by the δ function is the same as the path followed by the particle with the same initial condition. Parcel trajectories can be used, therefore, to construct the Green's function.

The following properties of the Green's function are worth noting. If the value of $\mathbf{x}_0$ is fixed, $\langle G(\mathbf{x}, \mathbf{x}_0, t) \rangle$ describes how air, initially at $\mathbf{x}_0$, disperses throughout the atmosphere as a function of t. Similarly, if the value of $\mathbf{x}$ is fixed, $\langle G(\mathbf{x}, \mathbf{x}_0, t) \rangle$ describes where the air located at $\mathbf{x}$ came from at earlier times. Thus, $\langle G(\mathbf{x}, \mathbf{x}_0, t) \rangle$ can be used to describe both where air goes and from where it comes.

3. Methods

a. General circulation model

In order to test the utility of these two approaches in a simplified but still realistic context, we use the wind field from an idealized general circulation model rather than observed winds. The model used is the National Center for Atmospheric Research Community Climate Model Version 2 (NCAR CCM2; Hack et al. 1993). Model integrations are carried out at T42 triangular truncation with 18 vertical levels. CCM2 uses a hybrid vertical coordinate referred to as η coordinates that transitions from a terrain-following sigma coordinate in the troposphere to pressure coordinates in the stratosphere (Hack et al. 1993). To improve the statistical sampling of the circulation, the boundary conditions and forcing are set as follows. The earth's surface has no topography, and there are no oceans. The entire surface is defined to be a single surface type (deciduous forest). The insolation is set to perpetual equinox conditions, so there is no seasonal cycle. Because of the zonally and hemispherically symmetric boundary conditions, and the lack of a seasonal cycle, there are no stationary waves or differences between the hemispheres other than those arising from the finite integration time. Because there are no oceans, the thermal relaxation time is on the order of a month.

The model is integrated for several years from an initial condition taken from a lower resolution simulation. The last two years of the simulation are used to provide three-dimensional winds for the calculations of air parcel trajectories.

b. Trajectory model

To compute the parcel trajectories, (1) is solved numerically using a standard fourth-order Runge–Kutta scheme (Bowman 1993) with 32 time steps per day and the discrete, three-dimensional velocity field from CCM2. Velocities at arbitrary $\mathbf{x}$ and t are computed by linear interpolation in space and time. Vertical motion is calculated in the model's η vertical coordinate system. At the top and bottom boundaries $\dot{\eta} = 0$. Although most global climate models, including CCM2, have a convective parameterization scheme, in this study we use only the large-scale vertical velocities computed from the continuity equation. As an example of the difficulties introduced by convective parameterizations when computing particle trajectories, consider a model grid box containing a particle. The location of the particle within the box is known. If the convective parameterization produces convective mass transport involving that box, does the particle participate in the convection, or is it in the part of the box where no convection occurs? Because convective parameterizations represent subgridscale processes, there is generally no knowledge of the spatial distribution of the convection within the grid box. Clearly convective transport plays an important role in the general circulation and trace species transport in both GCMs and the atmosphere. Here, we follow the philosophy of beginning with simple models and moving to more complex models as our understanding grows. The dual problems of representing convective transport in Lagrangian calculations and understanding the effects of convection on large-scale transport are left for later work. In this study, transport due to the convective parameterization scheme has been neglected.

In order that individual particles approximately represent equal masses of air, trajectories are initialized on a three-dimensional global grid that is equally spaced in longitude λ, sine of latitude μ, and altitude η. The grid size in longitude, latitude, and altitude is $36 \times 48 \times 20$, which yields a grid spacing of 10° longitude, ~2.4° to ~8.6° latitude (at the equator and ~80° latitude, respectively), and 50 hPa. Using two years of model output, trajectories are initialized at 5-day intervals and are integrated forward for 30 days. This gives 141 overlapping integrations.

c. Lagrangian statistics

Because of the zonal symmetry of the model boundary conditions and climate, the statistics can be averaged over longitude, increasing the sample size by a factor of 36. The hemispheric symmetry provides another factor of 2, so the sample size for each initial latitude and altitude is $141 \times 36 \times 2 = 10\,152$. The Lagrangian mean statistics are computed directly from the particle coordinates, although they could also be computed as the moments of the Green's functions.

d. Computing the Green's function

While the theoretical Green's function is defined everywhere, in practice $G(\mathbf{x}, \mathbf{x}_0, t)$ can only be evaluated at a finite number of initial locations $\mathbf{x}_0$, destination coordinates $\mathbf{x}$, and times t. The ensemble-mean Green's function for an ensemble of N realizations ($N = 141$ in this case) of $\mathbf{v}$ can be averaged over a finite subvolume within the domain to give

$$\langle G_i \rangle = \int_{\mathbf{x}_i} \langle G(\mathbf{x}, \mathbf{x}_0, t) \rangle \, d\mathbf{x} = \left\langle \int_{\mathbf{x}_i} G(\mathbf{x}, \mathbf{x}_0, t) \, d\mathbf{x} \right\rangle, \quad (9a)$$

where $\mathbf{x}_i$ is the portion of the domain within the ith subvolume. Consider the set of N solutions to (5) for a particular initial condition $\mathbf{x}_0$. By substituting for $G(\mathbf{x}, \mathbf{x}_0, t)$ from (8), it can easily be shown that

$$\langle G_i(\mathbf{x}_0, t) \rangle = \left\langle \int_{\mathbf{x}_i} \delta(\mathbf{x} - \mathbf{x}'(\mathbf{x}_0, t)) \, d\mathbf{x} \right\rangle = \frac{m_i(\mathbf{x}_0, t)}{N}, \quad (9b)$$

where m_i is the number of δ functions initially at $\mathbf{x}_0$ that are in the volume $\mathbf{x}_i$ at time t.

The Green's function is computed from the particle trajectories ($\mathbf{x}'$). For a particular initial condition $\mathbf{x}_0$, N trajectories are computed corresponding to the N realizations of the velocity field. As t increases, the trajectories spread out into a distribution in space. The distribution is characterized by dividing the domain into a regular array of grid boxes and counting the number of particles in each grid box, giving a distribution $p_i(\mathbf{x}_0, t) = n_i(\mathbf{x}_0, t)/N$, where n_i is the number of particles initially at $\mathbf{x}_0$ that are in grid box i at time t. Because of the correspondence between the trajectories and characteristics, $n_i = m_i$ and $p_i = \langle G_i \rangle$. Therefore, the probability distribution of particles provides a discrete approximation to the transport Green's function.

Because $\langle G \rangle$ is estimated by counting the number of particles in discrete bins, sampling errors could be important. Whether a particle falls into a particular bin can be viewed as a random process, so it is possible to obtain a simple quantitative estimate of the error of $\langle G_i \rangle$ from the binomial distribution. The standard deviation of the binomial distribution is $\sigma_i = \sqrt{p_i(1 - p_i)/n}$, where p_i is the probability that a particle will fall in the ith bin, and n is the total number of particles. If the particles are distributed across m bins, where $m \gg 1$, then $p_i \ll 1$ and $\sigma_i \cong \sqrt{p_i/n}$. The standard deviation relative to the mean is then $\sigma_i/p_i \cong \sqrt{1/(np_i)}$. If the particles are roughly uniformly distributed, so that $p_i \approx 1/m$, then $\sigma_i/p_i \cong \sqrt{m/n}$. Here we estimate two-dimensional (latitude–altitude) integrals of $\langle G \rangle$ using $\sim 10^4$ particles and $\sim 4 \times 10^2$ bins, which gives a relative error of ~20%. Examples below will demonstrate that, except near the edges of the particle distributions, where relative errors are large, $\langle G \rangle$ is smooth. This indicates that the sampling errors are acceptably small.

4. Results

a. Eulerian-mean circulation

For reference, Fig. 1 shows the Eulerian time-mean zonal-mean zonal wind $\overline{u}$ and the mean-meridional circulation ($\overline{v}$, $\dot{\overline{\eta}}$). The jet has realistic structure and magnitude, with a peak slightly greater than 40 m s^{-1} located near 200 hPa between 30° and 35° latitude. There are easterlies at the surface in the Tropics and in high latitudes. The mean-meridional circulation exhibits the classical three-cell structure, with a Hadley cell in the Tropics, a Ferrell cell in midlatitudes, and a weak polar cell in high latitudes.

b. Transport circulation in the latitude–altitude plane

Figure 2 shows the ensemble-mean Lagrangian velocity (2) in the latitude–altitude plane for averaging periods of 0.25, 1, 5, and 30 days. At short times (0.25 days) the Lagrangian velocity field is very similar to the Eulerian-mean velocity. By as early as 1 day, however, the two fields already differ significantly. The differences become more pronounced as the averaging period increases. After 5 days the Lagrangian-mean motion in the tropical lower troposphere is upward, but most other evidence of a tropical Hadley cell has disappeared. In the extratropics the mean motion is generally directed along slanting paths away from the boundaries and toward the middle troposphere. After 30 days the mean motion away from the boundaries toward the center of the domain completely dominates the Lagrangian velocities. The strong dependence of the Lagrangian-mean velocity on the averaging period and the

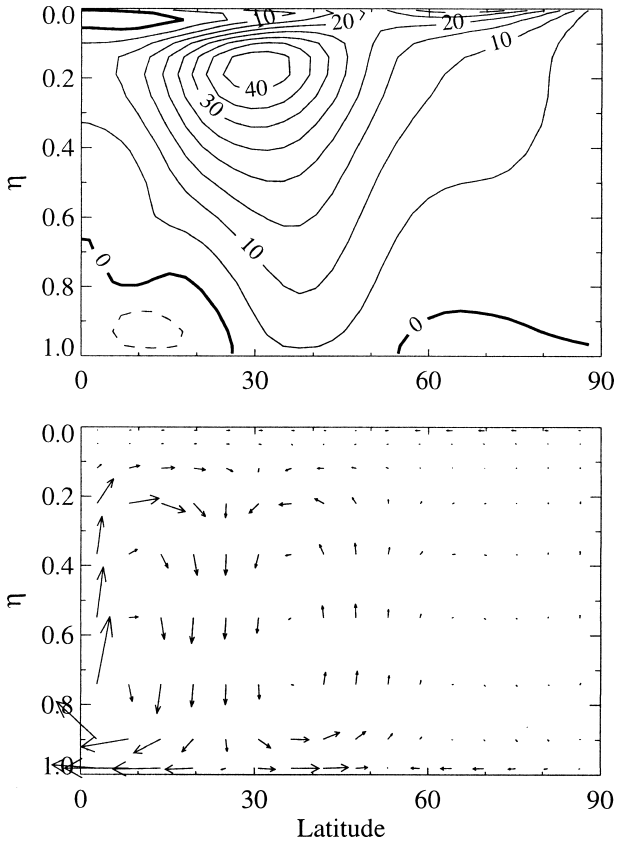

FIG. 1. Latitude–altitude cross sections of the time-mean zonal-mean zonal wind $\overline{u}$ (top) and the zonal-mean meridional and vertical components of the velocity (bottom). The vertical coordinate is η, which is the modified σ-like vertical coordinate used in CCM2.

importance of boundary effects indicate that simple Lagrangian-means may not provide a very useful picture of the mean-meridional transport circulation.

The reasons for the observed development of the Lagrangian-mean velocity field in the latitude–altitude plane can be seen by examining the dispersion of particles from different initial locations as a function of time. Figure 3 shows the distribution of particles from four different initial locations after 1.5 days. The intersection of the straight horizontal and vertical lines indicates the initial position of the particles, which is also given by the label in the upper left corner of each panel. Superimposed in black on each plot are contours of the time-mean zonal-mean potential temperature θ. Superimposed in white are contours of particle density. The white contours represent the discrete approximation to the Green's function $\langle G \rangle$ as estimated from the ensemble of particles.

Particles initialized in the equatorial lower troposphere (top left panel) rapidly disperse upward across the isentropes as they are caught in convection in the intertropical convergence zone (ITCZ). At this time the distribution is highly skewed. Most particles remain in the lower troposphere, but a long tail of particles extends upward all the way to the tropical tropopause. As a consequence, the mean particle displacement is upward. The mode (peak) of the distribution moves upward to about 875 hPa, which is considerably less than the mean displacement (discussed further below). Particles initialized in the extratropical middle troposphere (top-right panel), on the other hand, disperse into a roughly elliptical distribution with a major axis approximately parallel to the isentropes. At this time the particles have not yet felt the influence of the boundaries, so the dispersion is nearly symmetric and the mean and the mode are both displaced slightly downward and equatorward. The bottom two panels show the effects of the lower and polar boundaries. The lower-left panel shows that the most likely motion of particles initialized in the extratropical lower troposphere, as indicated by the shift in the peak of the distribution, is downward and equatorward. At the same time, many particles disperse upward and poleward into the free troposphere. As a result, the mean and the maximum likelihood particle displacements are in nearly opposite directions. Similar results hold for particles initialized in the polar upper troposphere (lower-right panel). The most likely displacement is slightly downward and equatorward, but the dispersion is asymmetric.

Figure 4 summarizes the displacement of the mean and mode for a large number of initial locations. Blue lines indicate the displacement of the mode or peak of the particle distributions, while the red lines indicate the displacements of the means of the distributions. In general, these two measures of the centers of the distributions disagree significantly, either in direction or in magnitude. Along the lower boundary, for example, the most likely motion is equatorward, which is across the mean isentropes toward higher potential temperatures (Held and Schneider 1999). The rapid, nearly isentropic dispersion away from the surface, however, results in skewed distributions that have mean displacements that are generally upward and poleward. In the ITCZ, on the other hand, the two displacements tend to be in the same direction (upward), but due to the skewness of the distributions the mean displacement is much larger than the most likely displacement.

As time increases, the particle distributions become more complicated and more difficult to characterize with a few parameters. Figure 5 shows the continued dispersion of particles initialized in the tropical lower troposphere. At 3 days, the distribution is distinctly bimodal. One group of particles has been carried to the tropical upper troposphere, while a second group has risen only into the lower to middle troposphere. Very few particles remain at low levels. As will be shown below, low-level tropical air is constantly replaced by air from the subtropics. After 10 days most of the particles are in the upper troposphere, and by 30 days the particles are well-mixed throughout the tropical troposphere. There is a relatively well-defined boundary between the Tropics and the extratropics. The

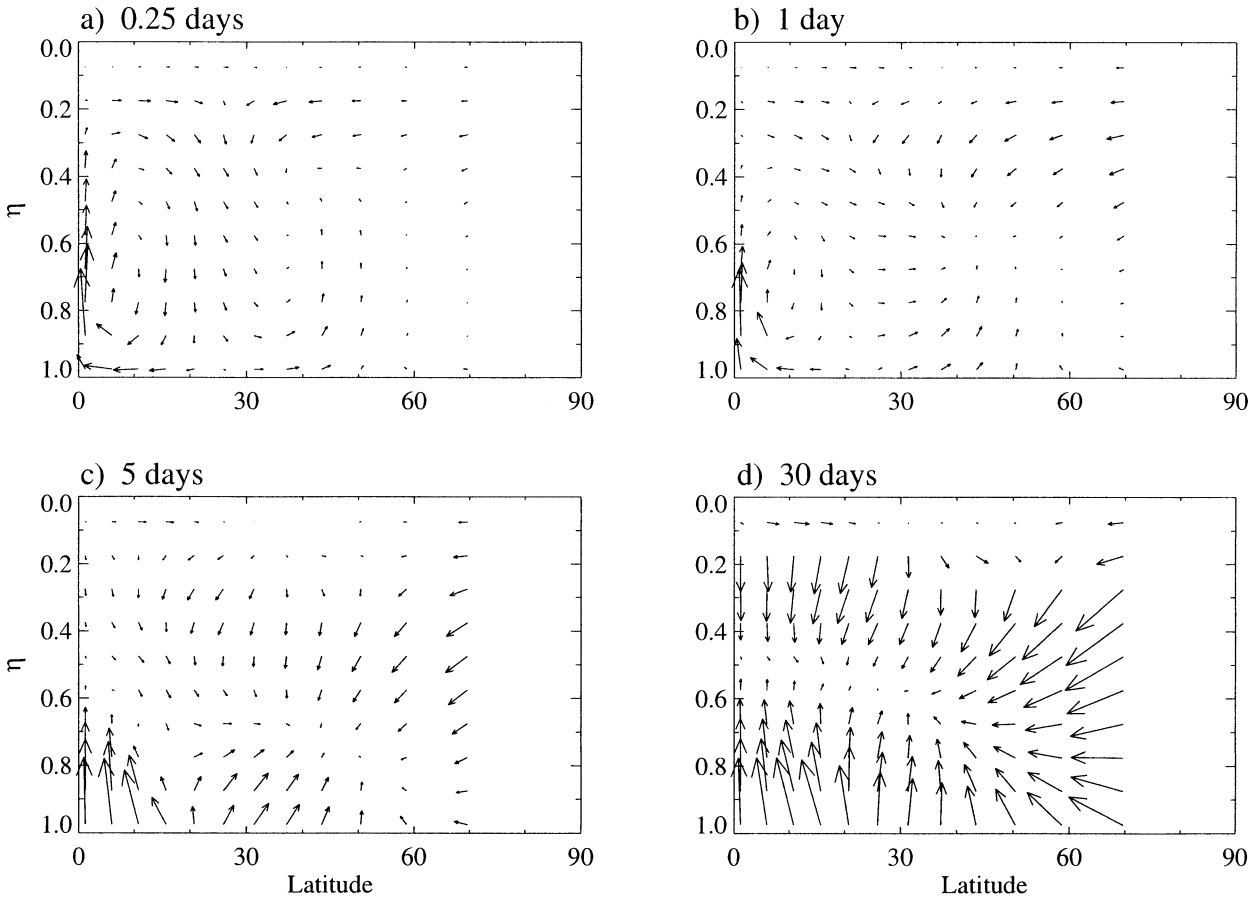

FIG. 2. Latitude–altitude cross sections of the Lagrangian-mean meridional and vertical velocities for averaging periods of 0.25, 1, 5, and 30 days.

boundary slopes poleward and upward from approximately 900 hPa at 15° latitude to 200 hPa at 40° latitude. Only a small percentage of the particles have moved into either the Northern or Southern Hemisphere extratropics.

Figure 6 shows a similar series of plots for particles initialized somewhat north of the equator in the tropical upper troposphere. These particles are most likely to initially move northward and downward. At the same time, some particles disperse southward throughout the tropical troposphere. There is some evidence of a weak transport barrier near the equator. Because the initial location was in the Northern Hemisphere, after 30 days most of the particles are still in the northern Tropics. Most of the particles have undergone substantial diabatic cooling. The distinct boundary between the Tropics and extratropics is again apparent.

Figure 7 illustrates the dispersion of particles in the extratropical troposphere. In this case, all particles initially between 43.4° and 58.7° latitude and between 575 and 675 hPa are included. The boundaries of the initial region are indicated by the pairs of horizontal and vertical lines. At 1 day the dispersion is roughly elliptic and oriented along the mean isentropes. As time progresses, particles descend into the boundary layer. These particles are heated and move equatorward at low levels toward higher potential temperatures. Once near the equator they are lofted into the tropical upper troposphere by the large-scale upward vertical motion (lower panels). The boundary or transport barrier between the Tropics and extratropics is visible as a gap between the two clouds of particles. By 20 days, those particles that have remained in the extratropics are relatively well-mixed throughout the extratropical troposphere.

For the initial condition of Fig. 7, the rate of transport into the Tropics and into the Southern Hemisphere extratropics is shown in Fig. 8. Each curve indicates the fraction of the particles within the latitude zones given in the labels. These zones are chosen to approximately represent the NH extratropics, the NH Tropics, and the SH Tropics. Because the boundary between the Tropics and extratropics slopes poleward with altitude, at low levels the extratropical troposphere extends to 15°–20° latitude. The rapid initial transport that occurs in the NH zones (up to about day 7) is due to particles moving into the subtropical lower troposphere, which is better considered to be part of the extratropical atmosphere. After about day 7, the transport changes to a nearly

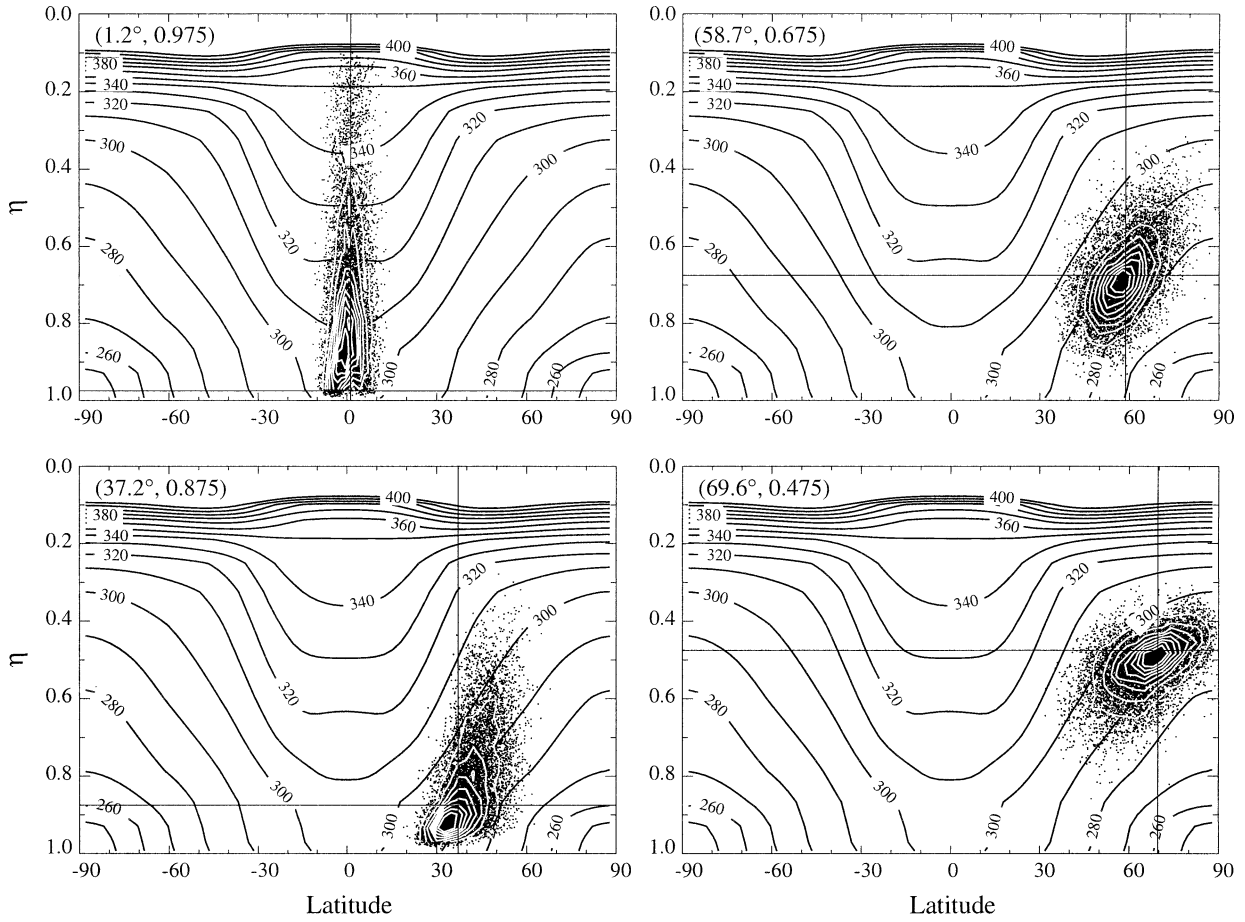

FIG. 3. Latitude–altitude cross sections of the dispersal of particle ensembles from four different initial conditions. In each panel the initial location of the particles is indicated by the intersecting vertical and horizontal lines. Black isopleths are the time-mean zonal-mean potential temperature. The white isopleths superimposed on the clouds of particles are particle density (Green's function) normalized by the maximum density. The contour interval is 0.1.

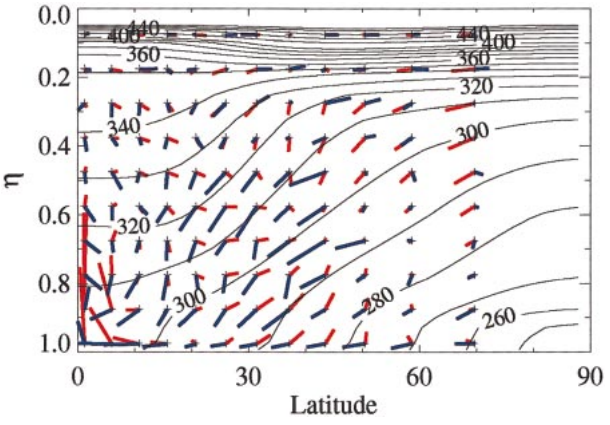

FIG. 4. The red and blue line segments indicate the mean and most likely displacement, respectively, of the ensemble of particles from each initial condition. Values are after 1.5 days of integration. The superimposed contours are the time-mean zonal-mean potential temperature.

steady flux of particles into the Tropics that can be considered to be ''true'' transport from the extratropics. From the nearly linear parts of the curves after day 7 it can be seen that the rate of transport from the extratropics into the Tropics is relatively slow. Between days 7 and 30, the NH extratropical atmosphere loses particles at an average rate of ~0.6%–0.7% per day. Within the Tropics, the transport across the equator itself is relatively quick. The fraction of particles transported into the SH extratropics is too small to be seen on this scale (<1% of the total on day 30). Similar calculations with particles initialized in the Tropics show that the particles first mix throughout the tropical troposphere and then move slowly into the middle latitudes at a rate of ~0.6% per day. This rate of transport is consistent with the rate of transport from the extratropics to the Tropics if the mass of the Tropics is approximately twice that of the mass of one hemisphere of the extratropical troposphere.

These results suggest that the following simple box model may be a useful tool for understanding global

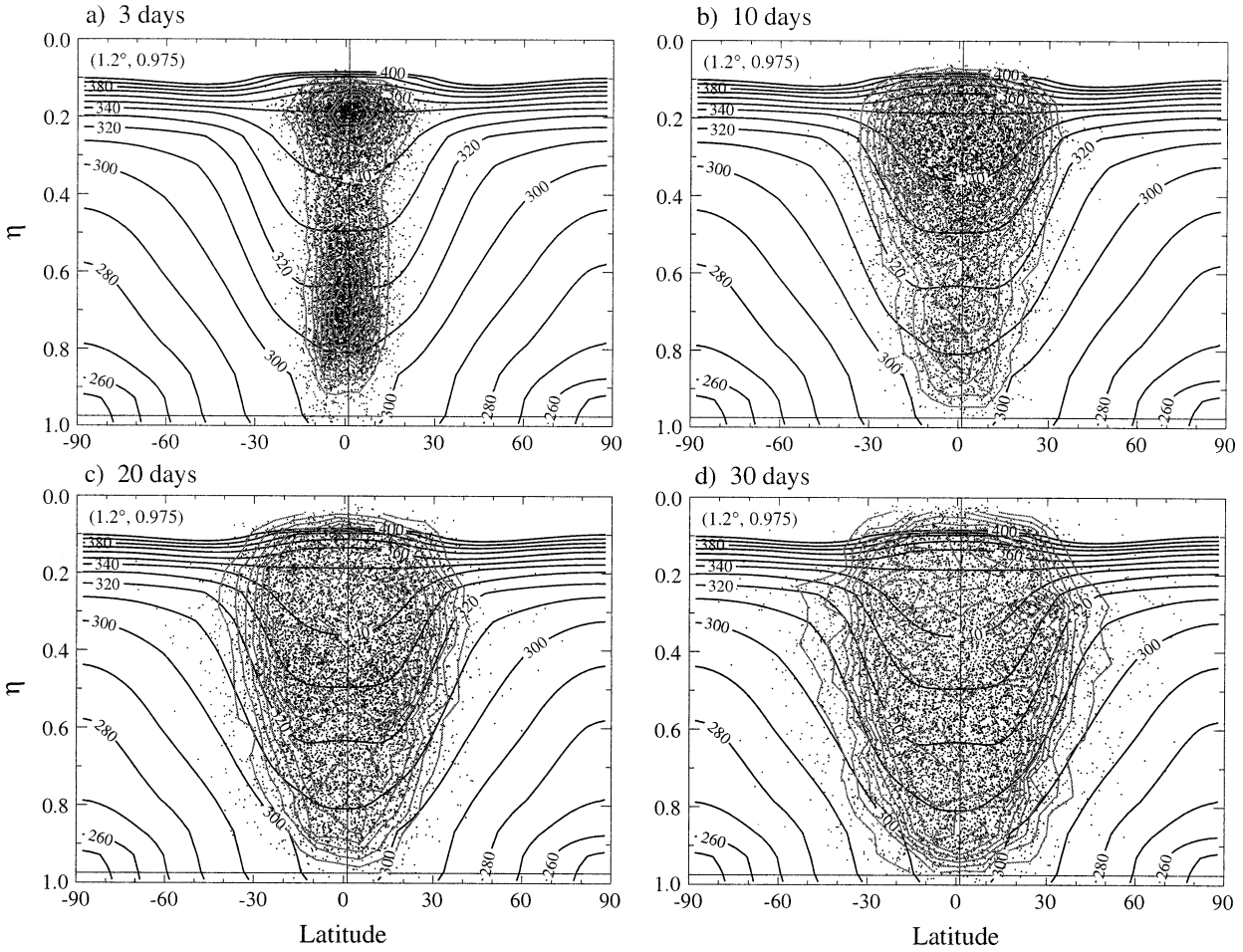

FIG. 5. Latitude–altitude cross sections of the dispersal of particle ensembles from a point in the tropical lower troposphere. In each panel the initial location of the particles is indicated by the intersecting vertical and horizontal lines. Heavy black isopleths are the time-mean zonal-mean potential temperature. The black isopleths superimposed on the clouds of particles are particle density (Green's function) normalized by the maximum density. The contour interval is 0.1.

transport. We take the troposphere to be divided into three boxes, two boxes of equal size in the southern and northern extratropics, and one box of twice that size in the Tropics (Fig. 9). The boxes are assumed to be well-mixed internally, and the tropical box exchanges air with the two extratropical boxes at equal and constant rates. The conservation equations for a conservative trace species in such a three-box model are

$$\frac{d\chi_S}{dt} = -r\chi_S + r\chi_T,$$

$$\frac{d\chi_T}{dt} = r\alpha\chi_S - 2r\alpha\chi_T + r\alpha\chi_N, \quad \text{and}$$

$$\frac{d\chi_N}{dt} = +r\chi_T - r\chi_N + S_N, \tag{10}$$

where χ_S, χ_T, and χ_N are the mass mixing ratios of tracer in the southern extratropical, tropical, and northern extratropical boxes respectively; r is the rate of mass exchange between the boxes divided by the mass of one of the extratropical boxes; α is the ratio of the mass in one of the extratropical boxes to the mass in the tropical box (taken here to be 0.5); and S_N represents a constant source of tracer in the Northern Hemisphere box. At large times, the effects of the initial conditions disappear, and the concentrations in each of the boxes increase at a constant rate, with the tropical and extratropical concentrations lagging that of the Northern Hemisphere box, which contains the source. The lags between the Northern Hemisphere and tropical boxes, and between the Northern and Southern Hemisphere boxes, are $(1 + \alpha)/\alpha r$ and $(1 + 2\alpha)/\alpha r$, respectively. A mass exchange rate r of 0.6% per day, as estimated from the Green's functions above, gives lags of ~1.4 and 1.8 yr for the tropical and Southern Hemisphere boxes, respectively. That is, the tropical box has the same tracer concentration that the northern extratropical box had ~1.4 yr earlier.

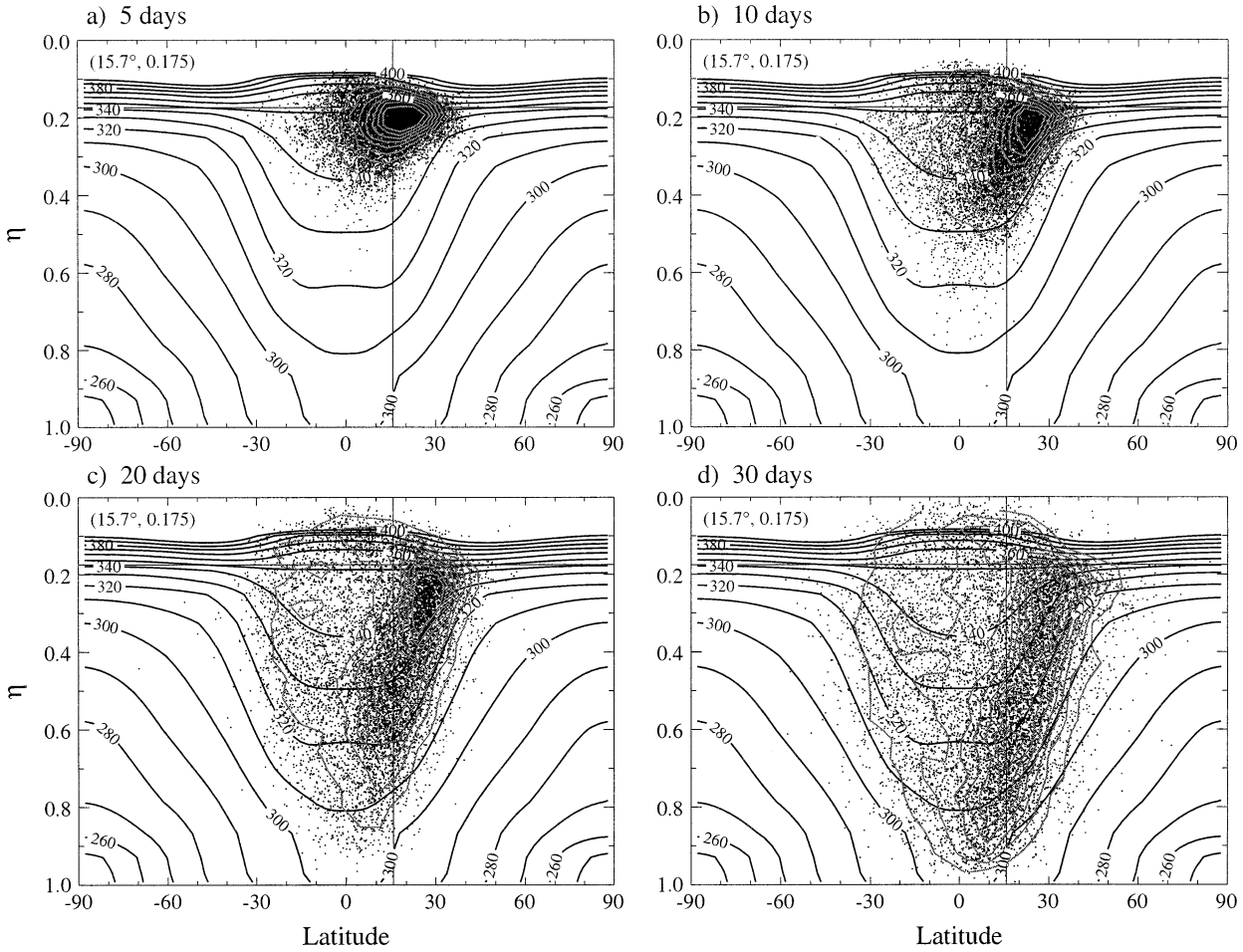

FIG. 6. As in Fig. 5, but for a point in the tropical upper troposphere.

c. Isentropic viewpoint

The initial dispersion of extratropical particles across the mean isentropes in Fig. 3 is due in part to the fact that particles initially at the same latitude and pressure may have varying potential temperatures. The cross-isentropic dispersion is thus not necessarily a result of diabatic heating or cooling, but of the potential temperature variations in the initial condition. The altitude of each particle can be converted to isentropic coordinates, which allows the Green's function to be computed in θ coordinates. The Green's function in θ coordinates is constructed by binning the initial locations of particles into latitude–θ bins and then computing the particle dispersion as a function of latitude and θ for each initial bin. An example of this analysis is shown in Fig. 10. In this case the latitude bins are the same size as the previous analyses, and particles are binned in 10-K bins in the vertical. The heavy-dashed line in Fig. 10 marks the mean potential temperature at the earth's surface. The dispersion of particles is shown from two initial locations, one in the tropical lower troposphere (dashed lines) and one in the extratropical middle troposphere (solid lines). As one would expect, in the Tropics, particles tend to undergo diabatic heating that raises them to higher potential temperatures. By contrast, in the extratropics particles tend to cool and move to lower potential temperatures. The low-level influx of extratropical air into the Tropics can be seen by examining the outermost solid contour in each panel. After 15 days the particles have largely mixed throughout the tropical and extratropical parts of the troposphere respectively, but there is little overlap between the two distributions. By 30 days some particles have ascended in the ITCZ, descended in the subtropical branch of the Hadley cell, and then mixed quasi-isentropically into the middle latitudes. A small fraction of the extratropical particles has also been mixed into the subtropics. This illustrates that the transport barrier between the Tropics and extratropics is not impermeable, but that transport through the barrier is significantly slower than mixing within either the tropical or extratropical parts of the troposphere.

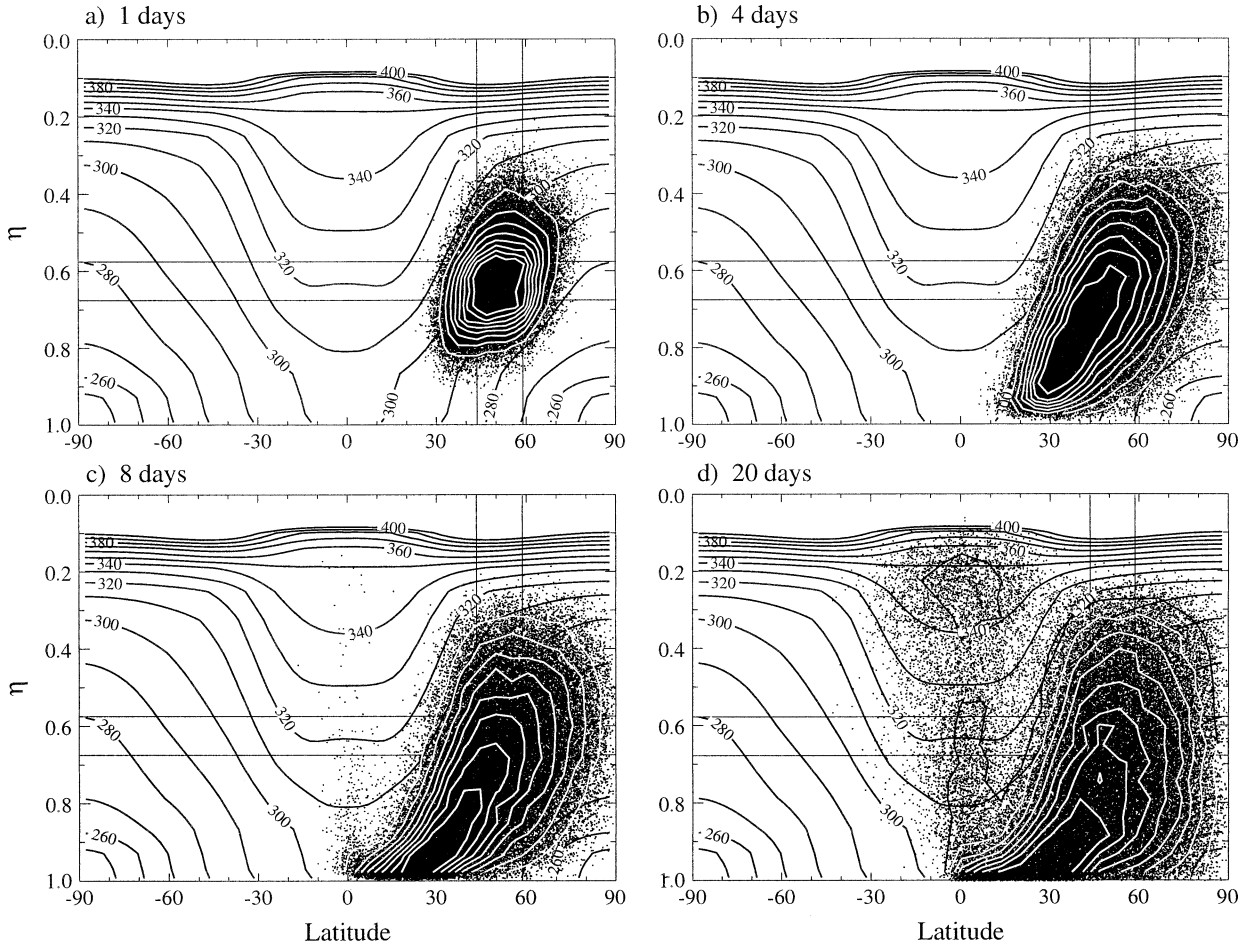

FIG. 7. As in Fig. 5, but for a rectangular initial condition in the extratropical middle troposphere. In this figure the particle density is shown in white, except for the lowest isopleth, which is black.

5. Discussion and conclusions

Here we have applied two different analysis methods to a large ensemble of air parcel trajectories in an idealized general circulation model in order to characterize the transport circulation of the model. While conceptually and computationally simple, Lagrangian-mean velocities can be difficult to use in practice because the distributions that they attempt to characterize are often highly skewed or even multimodal. In these circumstances, means do not provide a very useful description of the particle distributions. Instead of considering only the first few moments of a distribution, it appears to be more valuable to consider the complete shape of the distribution, or at least a discrete approximation to the distribution. We have shown that the probability distribution functions of Lagrangian particle trajectories are equivalent to the Green's function for the nondiffusive tracer advection equation. Therefore, a discrete approximation of the Green's function can be computed from an ensemble of Lagrangian trajectories. This Green's function provides a general solution to the climatological transport equation for an arbitrary initial distribution of tracer. The Green's function also provides a nice quantitative method that can be used to compare the transport circulation between two models, or between a model and atmospheric observations.

The Green's function approach has limitations, of course. In common with any analysis method, whether Eulerian or Lagrangian, it shares the limitations inherent in the observations or simulation. Those limitations include errors and uncertainties in wind observations, spatial and temporal resolution, etc. The Lagrangian approach also makes assumptions about the persistence of the identity of air parcels (Schoeberl et al. 2000). Additionally, it is necessary to have sufficient particles to provide good estimates of the Green's functions. Because it is possible to compute trajectories for large numbers of particles, in most cases this is not a serious constraint.

The transport circulation in the latitude–altitude plane in our idealized GCM is summarized in the schematic in Fig. 11. The black arrows indicate the primary sense of the transport, while the crossed gray arrows indicate the relative magnitude of the dispersion of air parcels.

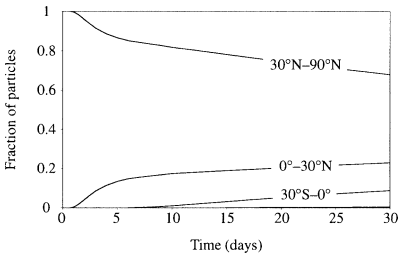

FIG. 8. For the initial condition shown in Fig. 7, this graph shows the fraction of particles in each of three latitude zones. The number of particles in the zone south of 30°S is too small to be seen in this plot.

The wide light-gray bands indicate the approximate location of the transport barriers between the Tropics and extratropics. Figure 11 has similarities to Fig. 8 in Kida (1983) and Fig. 18 in Plumb and Mahlman (1987). The most important difference in the current work is the identification of a clear transport barrier between the Tropics and extratropics. It is important to remember, however, that this model is much more zonally symmetric than the real atmosphere due to the lack of topography and land–sea contrast. In the Tropics there is a Hadley-like circulation with convergence toward the equator at low levels, rising motion along the equator, divergent poleward motion from the equator in the upper troposphere, and subsidence in the subtropics. Much of this air does recirculate in the Tropics, but some moves through the transport barrier into the extratropics, replacing extratropical air that moves into the Tropics in the low-level trade-wind circulation. Air parcels disperse horizontally throughout the Tropics relatively quickly. Air that begins in the tropical lower troposphere mixes nearly uniformly throughout the Tropics on a timescale of about a month. Air that begins in the subsiding branch of the tropical circulation requires somewhat longer.

In the extratropics air parcels disperse relatively rapidly both along and across isentropes. Boundaries have a strong effect on the shapes of the particle distributions and the mean motion of particles. At low levels, air moves equatorward across the isentropes toward higher potential temperatures. In synoptic terms, air that moves equatorward behind a cold front tends to have potential temperatures lower than the zonal average. This air is heated by contact with the surface and moves equatorward to warmer potential temperatures. As Held and Schneider (1999) noted, much of the equatorward branch of the mean overturning circulation occurs ''underground.'' That is, below the mean potential temperature of the earth's surface. When this air nears the equator it ascends into the tropical upper troposphere.

The transport barrier between the Tropics and extratropics clearly cannot be impermeable. The entrainment of extratropical air into the Tropics in the boundary layer must be matched in the long term by transport of air from the Tropics back into the extratropics through the transport barrier. It is important to remember also that subgridscale convective transport has been neglected when computing vertical motion of particles. The role of subgridscale convective motion will be addressed in later work.

This picture of the global transport circulation is consistent with some atmospheric chemical data, such as the measurements of long-lived man-made chemicals like CFC-12 (CF_2Cl_2) from the Atmospheric Lifetime Experiment (ALE) and the Global Atmospheric Gases Experiment (GAGE; Prinn et al. 1983; Cunnold et al. 1994; Fraser et al. 1996). Until the mid-1990s, the concentration of CFC-12 increased steadily in the atmosphere due to a comparatively long lifetime and continued release into the atmosphere. Gases such as CFC-12 were primarily released into the atmosphere in the Northern Hemisphere extratropics. Long-term measurements show that during the period of increasing atmospheric CFC concentrations, subtropical Northern Hemisphere stations such as Barbados, lagged only

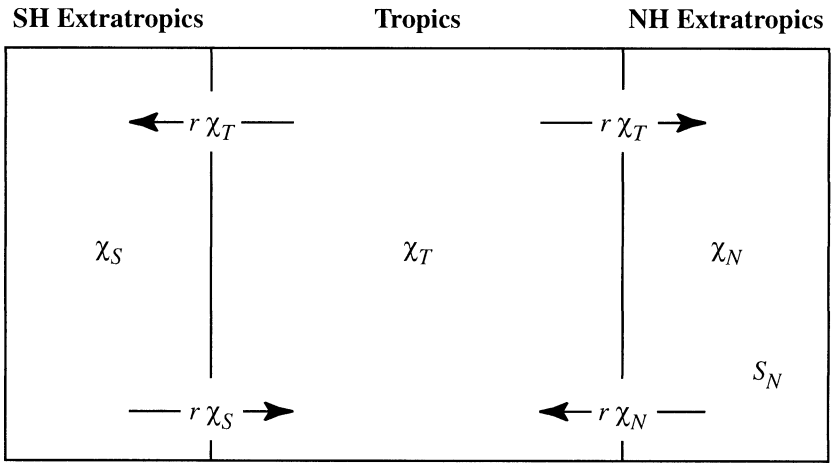

FIG. 9. Schematic of the three-box model showing the transport pathways.

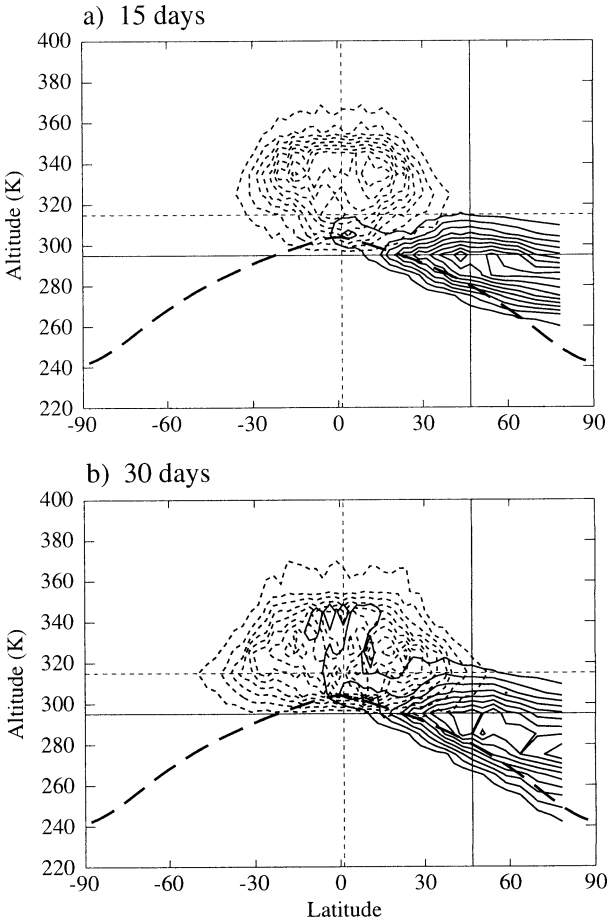

FIG. 10. Latitude–θ cross sections of the particle density (Green's function) normalized by the maximum density after 15 and 30 days. The contour interval is 0.1. Two initial conditions are shown in each panel, one in the tropical lower troposphere (dashed isopleths) and one in the extratropical middle troposphere (solid isopleths).

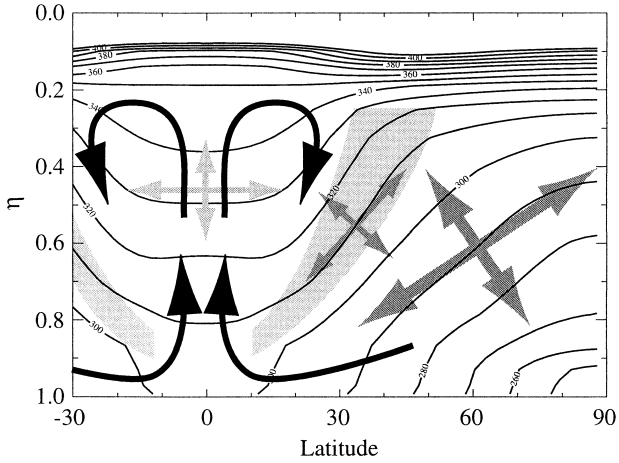

FIG. 11. Schematic of the transport circulation in this CCM2 simulation, which has no topography or land–sea contrast and perpetual equinox insolation. Semipermeable transport barriers in the subtropics, indicated by gray shading, separate the troposphere into three regions: the southern extratropics, the Tropics, and the northern extratropics. Black arrows indicate a well-defined transport circulation. Crossed gray arrows qualitatively indicate mixing rates and preferred directions.

slightly behind midlatitude stations in Ireland and Oregon (see Fig. 1 in Bowman and Cohen 1997). Southern Hemisphere tropical and extratropical stations also tended to have similar levels of CFC-12 with each other, but there was a significant gap between the Northern and Southern Hemisphere stations. This is consistent with the transport processes outlined in Fig. 11. Long-lived trace species released at the surface in the Northern Hemisphere extratropics mix throughout the extratropical troposphere on a timescale of a few weeks. On a slower timescale they are transported into the Tropics in the boundary layer and then mixed throughout the tropical troposphere. Transport out of the Tropics into either the Northern or Southern Hemispheres is also relatively slow. Because of the comparatively slow exchange of air between the Tropics and extratropics, observed CFC-12 concentrations in the Southern Hemisphere extratropical troposphere lagged approximately 1 yr behind those in the Northern Hemisphere. The timescale for interhemispheric exchange estimated from the trace gas data is 1 to 2 yr, depending on which stations are used. The lag estimated from CCM2 using the particle trajectories is ~1.8 yr, which is within the range of values found in the observations.

The Eulerian mean–meridional mass circulation can be computed in isentropic coordinates, which have many of the properties of the transformed Eulerian coordinate system (Townsend and Johnson 1985; Held and Schneider 1999). Unlike the conventional three-celled Eulerian-mean circulation, the isentropic Eulerian-mean circulation is comprised of a single thermally direct cell that spans the entire hemisphere. It is tempting to think of this mean circulation as the transport circulation, but that interpretation should be made with some caution. The dominant features of the transport circulation visible in the Green's function are the rapid dispersion within the extratropical and tropical parts of the atmosphere and the comparatively slow interchange between those parts. The isentropic-mean mass circulation may capture the second part of that transport, but not the first.

The transport barriers between the Tropics and extratropics appear to be largely responsible for the comparatively long transport timescale between the Northern and Southern Hemispheres. These results suggest that global chemical transport models may require high-fidelity simulations of the subtropical interface between the rapid quasi-isentropic mixing by eddies in the extratropics and the diabatic overturning of the tropical Hadley circulation.

Acknowledgments. This research made use of the Community Climate Model Version 2 (CCM2) from the National Center for Atmospheric Research (NCAR).

The authors gratefully acknowledge the CCM project. This research was funded in part by NASA Grant NAG-1-1896 to Texas A&M University. The authors also thank the reviewers for their comments and suggestions.

REFERENCES

Andrews, D. G., 1983: A finite-amplitude Eliassen–Palm theorem in isentropic coordinates. *J. Atmos. Sci.,* **40,** 1877–1883.

——, and M. E. McIntyre, 1976: Planetary waves in horizontal and vertical shear: The generalized Eliassen–Palm relation and the mean zonal acceleration. *J. Atmos. Sci.,* **33,** 2031–2048.

——, and ——, 1978a: An exact theory of nonlinear waves on a Lagrangian-mean flow. *J. Fluid Mech.,* **89,** 609–646.

——, and ——, 1978b: Generalized Eliassen–Palm and Charney–Drazin theorems for waves on axisymmetric mean flows in compressible atmospheres. *J. Atmos. Sci.,* **35,** 175–185.

——, J. R. Holton, and C. B. Leovy, 1987: *Middle Atmosphere Dynamics.* Academic Press, 489 pp.

Austin, J., and A. F. Tuck, 1985: The calculation of stratospheric air parcel trajectories using satellite data. *Quart. J. Roy. Meteor. Soc.,* **111,** 279–307.

Bowman, K. P., 1993: Large-scale isentropic mixing properties of the Antarctic polar vortex from analyzed winds. *J. Geophys. Res.,* **98,** 23 013–23 027.

——, 1996: Rossby wave phase speeds and mixing barriers in the stratosphere. Part I: Observations. *J. Atmos. Sci.,* **53,** 905–916.

——, and P. J. Cohen, 1997: Interhemispheric exchange by seasonal modulation of the Hadley circulation. *J. Atmos. Sci.,* **54,** 2045–2059.

Boyd, J. P., 1976: The noninteraction of waves with the zonally averaged flow on a spherical earth and the interrelationships of eddy fluxes of energy, heat and momentum. *J. Atmos. Sci.,* **33,** 2285–2291.

Chen, P., 1994: The permeability of the Antarctic vortex edge. *J. Geophys. Res.,* **99,** 20 563–20 571.

Cunnold, D. M., P. J. Fraser, R. F. Weiss, R. G. Prinn, P. G. Simmonds, B. R. Miller, F. N. Alyea, and A. J. Crawford, 1994: Global trends and annual releases of CCl_3F and CCl_2F_2 estimated from ALE/GAGE and other measurements from July 1978 to June 1991. *J. Geophys. Res.,* **99,** 1107–1126.

Dunkerton, T. J., 1978: On the mean meridional mass motions of the stratosphere and mesosphere. *J. Atmos. Sci.,* **35,** 2325–2333.

Fisher, M., A. O'Neill, and R. Sutton, 1993: Rapid descent of mesospheric air into the stratospheric polar vortex. *Geophys. Res. Lett.,* **20,** 1267–1270.

Fraser, P., D. Cunnold, F. Alyea, R. Weiss, R. Prinn, P. Simmonds, B. Miller, and R. Langenfelds, 1996: Lifetime and emission estimates of 1,1,2-trichlorotriflourethane (CFC-113) from daily global background observations June 1982–June 1994. *J. Geophys. Res.,* **101,** 12 585–12 599.

Hack, J. J., B. A. Boville, B. P. Briegleb, J. T. Kiehl, P. J. Rasch, and D. L. Williamson, 1993: Description of the NCAR Community Climate Model (CCM2). NCAR Tech. Note NCAR/TN-382+STR, 108 pp.

Hall, T. M., and R. A. Plumb, 1994: Age as a diagnostic of stratospheric transport. *J. Geophys. Res.,* **99,** 1059–1070.

Held, I. M., and T. Schneider, 1999: The surface branch of the zonally averaged mass transport circulation in the troposphere. *J. Atmos. Sci.,* **56,** 1688–1697.

Holzer, M., 1999: Analysis of passive tracer transport as modeled by an atmospheric general circulation model. *J. Climate,* **12,** 1659–1684.

Hsu, C.-P. F., 1980: Air parcel motions during a numerically simulated sudden stratospheric warming. *J. Atmos. Sci.,* **37,** 2768–2792.

Kida, H., 1983: General circulation of air parcels and transport characteristics derived from a hemispheric GCM. Part 2. Very long-term motions of air parcels in the troposphere and stratosphere. *J. Meteor. Soc. Japan,* **61,** 510–522.

Matsuno, T., 1980: Lagrangian motion of air parcels in the stratosphere in the presence of planetary waves. *Pure Appl. Geophys.,* **118,** 189–216.

Oort, A. H., and E. M. Rasmusson, 1971: *Atmospheric Circulation Statistics.* United States Dept. of Commerce, 323 pp.

Pierce, R. B., and T. D. A. Fairlie, 1993: Chaotic advection in the stratosphere: Implications for the dispersal of chemically perturbed air from the polar vortex. *J. Geophys. Res.,* **98,** 18 589–18 595.

Pierrehumbert, R. T., and H. Yang, 1993: Global chaotic mixing on isentropic surfaces. *J. Atmos. Sci.,* **50,** 2462–2480.

Plumb, R. A., and J. D. Mahlman, 1987: The zonally averaged transport characteristics of the GFDL general circulation/transport model. *J. Atmos. Sci.,* **44,** 298–327.

Prinn, R., and Coauthors, 1983: The Atmospheric Lifetime Experiment. I: Introduction, instrumentation and overview. *J. Geophys. Res.,* **88,** 8353–8368.

Schoeberl, M. R., L. R. Lait, P. A. Newman, and J. E. Rosenfield, 1992: The structure of the polar vortex. *J. Geophys. Res.,* **97,** 7859–7882.

——, L. C. Sparling, C. H. Jackman, and E. L. Fleming, 2000: A Lagrangian view of stratospheric trace gas distributions. *J. Geophys. Res.,* **105,** 1537–1552.

Stone, E. M., W. J. Randel, and J. L. Stanford, 1999: Transport of passive tracers in baroclinic wave life cycles. *J. Atmos. Sci.,* **56,** 1364–1381.

Sutton, R. T., H. Maclean, R. Swinbank, A. O'Neill, and F. W. Taylor, 1994: High-resolution stratospheric tracer fields estimated from satellite observations using Lagrangian trajectory calculations. *J. Atmos. Sci.,* **51,** 2995–3005.

Townsend, R. D., and D. R. Johnson, 1985: A diagnostic study of the isentropic zonally averaged mass circulation during the First GARP Global Experiment. *J. Atmos. Sci.,* **42,** 1565–1579.